

Invariant curves near Hamiltonian-Hopf bifurcations of 4D symplectic maps

Àngel Jorba⁽¹⁾ and Mercè Ollé⁽²⁾

30th January 2003

- (1) Departament de Matemàtica Aplicada i Anàlisi, Universitat de Barcelona, Gran Via 585, 08007 Barcelona, Spain. E-mail: angel@maia.ub.es
- (2) Department de Matemàtica Aplicada I, Universitat Politècnica de Catalunya, Diagonal 647, 08028 Barcelona, Spain. E-mail: merce.olle@upc.es

Abstract

In this paper we give a numerical description of the neighbourhood of a fixed point of a symplectic map undergoing a transition from linear stability to complex instability, i.e., the so called Hamiltonian-Hopf bifurcation. We have considered both the direct and inverse cases.

The study is based on the numerical computation of the Lyapunov families of invariant curves near the fixed point. We show how these families, jointly with their invariant manifolds and the invariant manifolds of the fixed point organise the phase space around the bifurcation.

Keywords: Complex instability, invariant curves, invariant manifolds.

Contents

1	Introduction	3
2	The model maps	4
2.1	Basic properties	4
3	Direct bifurcation	6
3.1	The Lyapunov families of invariant curves	7
3.2	Complex unstable fixed points. Invariant manifolds	8
3.3	Unfolding of tori. Hopf bifurcation	12
3.4	Confinement. Invariant curves and 2D tori	14
4	Inverse bifurcation	15
4.1	The Lyapunov families of invariant curves	18
4.2	Invariant manifolds	19
5	Summary of numerical methods	20
5.1	Invariant curves	21
5.2	Linear normal behaviour around invariant curves	22
5.3	Invariant manifolds	23
5.3.1	Manifolds of a complex unstable fixed point	23
5.3.2	Manifolds of an invariant curve	24
	References	25

1 Introduction

In this paper we focus on the dynamics near a fixed point of a one-parametric family of four-dimensional symplectic maps, in the case in which the fixed point undergoes a transition to complex instability (also known as Hamiltonian-Hopf bifurcation). This bifurcation can be briefly described as follows. On one side of the bifurcation the fixed point is linearly stable, this is, all the eigenvalues of the Jacobian matrix at the point have modulus one. Due to the conditions imposed by the symplectic structure, these eigenvalues come in two couples of conjugate complex numbers, that move on the unit circle when we move along the family. When we approach the bifurcation, the two pairs come close in such a way that, at the bifurcation point, they collapse in a single pair of complex eigenvalues (the collapse occurs on the unit circle but outside the real line). After that, the four eigenvalues separate and move off the unit circle (two move outside and two move inside the unit disc) and the point becomes unstable. As none of the eigenvalues is real, the real stable and unstable manifolds are two-dimensional and, near the fixed point, the orbits inside them spiral in and out respectively.

It is also well-known that the dynamics of a Hamiltonian system can be analysed through the behaviour of the iterates of a suitable symplectic Poincaré map. In this sense, the maps considered here can also be seen as a model for the transition to complex instability of a periodic orbit of a three degrees of freedom Hamiltonian system.

From an analytical point of view, the transition to complex instability has been studied using the Hamiltonian itself (see [Heg85], [OPV], [Pac02]) or the 4D symplectic mapping (see [BCM95]). In both cases, the approach consists of normal form techniques to simplify the Hamiltonian (or the map) and describe the local phase space structure near the critical periodic orbit (or fixed point in the discrete context). Such analysis shows that the transition to complex instability gives rise to bifurcating invariant 2D tori in the flow context, or invariant curves in case of mappings. It is remarkable that there exists not one but two kinds of Hamiltonian-Hopf bifurcations (as it happens in the usual –dissipative– setting), depending on the nonlinear terms. This is clearly seen from the normal forms (see, for instance, [Mee85]). These two kinds of bifurcations are usually called direct and inverse. We should also cite the works [Pfe85a], [CG88] and [Oll00], that contain numerical computations related to some aspects of this bifurcation.

The goal of this paper is to give a local geometrical picture of the dynamics close to an elliptic, critical or complex unstable fixed point, without any reduction to normal form. To do so, we consider two families of nonlinear symplectic 4D mappings T_s and T_t , which can also be thought of as suitable Poincaré maps of a generic three degree of freedom Hamiltonian system. Both families of mappings have the origin as fixed point, with a transition from stability to complex instability as we move along the families (in T_s , the bifurcation is a direct Hopf, while in T_t it is an inverse one). The dynamics of the mappings T_s and T_t , and its invariant curves will be used as a model to describe the Hamiltonian Hopf bifurcation in both cases.

Our approach is based on numerical computations of the main invariant objects around the bifurcation –invariant curves and invariant manifolds– for the model mappings T_s and T_t . More concretely, when the origin of these maps is linearly stable, we compute the

Lyapunov families of invariant curves that are born at the origin and, if they are hyperbolic, we also compute the stable and unstable manifolds. When the origin is complex unstable, we compute its stable and unstable manifolds. The study of the behaviour of these objects in the transition to complex instability allows for a geometrical description of the phase space around the bifurcation.

In real problems, such bifurcation appears, for example, in the restricted three-body problem (see [OP99a], [OP98a]), in the problem of the stability of planetary systems ([Had85]), or in galactic dynamics (see [Pfe85b], [Pfe90], [CB94], [OP98b] and references therein).

The paper is organised as follows. In Section 2 we introduce the mappings T_s and T_t and we discuss some of their basic properties. Section 3 is devoted to the analysis of the Hamiltonian-Hopf bifurcation for T_s (direct case) and Section 4 for the mapping T_t (inverse case). The numerical methods used have been summarised in Section 5.

2 The model maps

Here we will focus on two maps, which can be seen as generalisations of the well-known standard map. They are defined by

$$T_s \begin{pmatrix} x_1 \\ x_2 \\ x_3 \\ x_4 \end{pmatrix} = \begin{pmatrix} x_1 + K_1 \sin(x_1 + x_2) + L_1 \sin(x_1 + x_2 + x_3 + x_4) \\ x_1 + x_2 \\ x_3 + K_2 \sin(x_3 + x_4) + L_2 \sin(x_1 + x_2 + x_3 + x_4) \\ x_3 + x_4 \end{pmatrix}$$

and

$$T_t \begin{pmatrix} x_1 \\ x_2 \\ x_3 \\ x_4 \end{pmatrix} = \begin{pmatrix} x_1 + K_1 \sin(x_1 + x_2) + L_1 \tan(x_1 + x_2 + x_3 + x_4) \\ x_1 + x_2 \\ x_3 + K_2 \sin(x_3 + x_4) + L_2 \tan(x_1 + x_2 + x_3 + x_4) \\ x_3 + x_4 \end{pmatrix}$$

Such mappings were used in [Fro72] (with $L_1 = L_2$) for exploring the properties of three degrees of freedom systems, and were also used in [Pfe85a] and [OP99b] (with $L_1 + L_2 = 0$) to give a first numerical insight of the Hamiltonian Hopf bifurcation.

2.1 Basic properties

The origin $x = (x_1, x_2, x_3, x_4) = 0$ is a fixed point of both mappings, for any value of the parameters K_1 , K_2 , L_1 and L_2 . The two mappings have the same Jacobian A around $x = 0$, but different non-linear behaviour as we will show below. The Jacobian A reads

$$A = \begin{pmatrix} 1 + K_1 + L_1 & K_1 + L_1 & L_1 & L_1 \\ 1 & 1 & 0 & 0 \\ L_2 & L_2 & 1 + K_2 + L_2 & K_2 + L_2 \\ 0 & 0 & 1 & 1 \end{pmatrix}.$$

A straightforward calculation shows that, if $L_1 + L_2 = 0$, T_s and T_t are symplectic mappings if the canonically conjugated variables are (x_1, x_2) and (x_4, x_3) . Therefore, from now on, we will assume that $L_1 + L_2 = 0$.

The characteristic polynomial of A has the form

$$z^4 + \alpha z^3 + \beta z^2 + \alpha z + 1 = (z^2 + b_1 z + 1)(z^2 + b_2 z + 1),$$

where the stability parameters b_1 , b_2 and Δ are defined by

$$b_1 = -\left(\lambda + \frac{1}{\lambda}\right), \quad b_2 = -\left(\mu + \frac{1}{\mu}\right), \quad \Delta = (b_1 + b_2)^2,$$

being λ , $1/\lambda$, μ , $1/\mu$ the eigenvalues of the (symplectic) matrix A , and α , β , b_1 and b_2 are related by

$$\alpha = b_1 + b_2, \quad \beta = 2 + b_1 b_2.$$

It is well known that $x = 0$ is (linearly) stable if $|b_1| \leq 2$, $|b_2| \leq 2$ and $\Delta \geq 0$, and complex unstable when $\Delta < 0$. A simple computation leads to

$$\begin{aligned} \alpha &= -(4 + K_1 + K_2), \\ \beta &= 6 + 2(K_1 + K_2) + K_1 L_2 + K_2 L_1 + K_1 K_2, \\ \Delta &= (K_1 - K_2 + L_1 - L_2)^2 + 4L_1 L_2. \end{aligned}$$

We restrict the parameter space by taking $K_2 = 0$ and $L_1 = -L_2 \stackrel{\text{def}}{=} L$. Renaming $K_1 = K$ we have that $\Delta = K(K + 4L)$. By inspection of Broucke's diagram of stability (that shows the behaviour of the eigenvalues of A according to α and β , see for example [Pfe85a]) and for $-8 < K < 0$ the transition ($\Delta = 0$) from stability to complex instability with respect to the parameter L takes place for the critical value $L_{crit} = -K/4$.

In particular, when $L = L_{crit}$ the Jacobian A becomes

$$A_{crit} = \begin{pmatrix} 1 + \frac{3}{4}K & \frac{3}{4}K & -\frac{K}{4} & -\frac{K}{4} \\ 1 & 1 & 0 & 0 \\ \frac{K}{4} & \frac{K}{4} & 1 + \frac{K}{4} & \frac{K}{4} \\ 0 & 0 & 1 & 1 \end{pmatrix},$$

with $-8 < K < 0$. Then, it follows that $\text{Spec}(A_{crit}) = \{\lambda, \bar{\lambda}\}$, being

$$\lambda = 1 + \frac{1}{4}K + i\frac{1}{4}\sqrt{8|K| - K^2},$$

and a corresponding eigenvector is

$$u + i v = \left(\frac{K + i\sqrt{8|K| - K^2}}{4}, 1, \frac{K + i\sqrt{8|K| - K^2}}{4}, 1 \right)^T.$$

Therefore, the real 2D plane generated by the (real) vectors u and v is invariant for the linear mapping defined by A_{crit} . Since $u_1 = u_3$, $v_1 = v_3$, $u_2 = u_4$ and $v_2 = v_4$, such invariant plane becomes $x_1 = x_3$, $x_2 = x_4$.

We also want to note that both mappings satisfy the following symmetry:

$$T_i(-x) = -T_i(x) \quad \text{for } i = s, t,$$

and that there exists a closed expression for the inverse of both,

$$T_s^{-1} \begin{pmatrix} x_1 \\ x_2 \\ x_3 \\ x_4 \end{pmatrix} = \begin{pmatrix} x_1 - K_1 \sin x_2 - L_1 \sin(x_2 + x_4) \\ x_2 - x_1 - K_1 \sin x_2 + L_1 \sin(x_2 + x_4) \\ x_3 - K_2 \sin x_4 - L_2 \sin(x_2 + x_4) \\ x_4 - x_3 + K_2 \sin x_4 + L_2 \sin(x_2 + x_4) \end{pmatrix},$$

$$T_t^{-1} \begin{pmatrix} x_1 \\ x_2 \\ x_3 \\ x_4 \end{pmatrix} = \begin{pmatrix} \frac{x_1 \cos(x_2 + x_4) - K_1 \sin x_2 \cos(x_2 + x_4) - L_1 \sin(x_2 + x_4)}{K_1 \sin x_2 \cos(x_2 + x_4) + L_1 \sin(x_2 + x_4) + (x_2 - x_1) \cos(x_2 + x_4)} \\ \frac{D}{D} \\ f(x_1, x_2, x_3, x_4) \\ g(x_1, x_2, x_3, x_4) \end{pmatrix},$$

with

$$f = -\frac{1}{D} ((K_2 \cos x_4 + L_2) \sin x_4 \cos x_2 - K_2 \sin x_2 + K_2 \sin x_2 \cos^2 x_4 + L_2 \sin x_2 \cos x_4 - x_3 \cos x_2 \cos x_4 + x_3 \sin x_2 \sin x_4), \quad (1)$$

$$g = -\frac{1}{D} (K_2 \sin x_2 - K_2 \sin x_2 \cos^2 x_4 - L_2 \sin x_2 \cos x_4 - L_2 \cos x_2 \sin x_4 + (x_3 - x_4 - K_2 \sin x_4)(\cos x_2 \cos x_4) + (x_4 - x_3) \sin x_2 \sin x_4), \quad (2)$$

and

$$D = \cos(x_2 + x_4).$$

Finally we note that, although T_t is not a one-to-one map of \mathbb{R}^4 , it is a local diffeomorphism around $x = 0$. This will be enough for our computations.

3 Direct bifurcation

Corresponds to the map T_s . To proceed with the numerical study, we will fix the value $K = -1$. Similar results are obtained with values $-8 < K < 0$.

We can briefly describe this bifurcation as follows. For $L < L_{crit}$, there are plenty of 2D invariant tori around the origin. When L crosses L_{crit} , the origin becomes hyperbolic and the (2D) unstable and stable manifolds are almost coincident so that they look like a small “loop”, its size depending on the size of $L - L_{crit} > 0$. Therefore, although the origin is unstable, the nearby trajectories are trapped¹ in a small neighbourhood. When L gets bigger, the “loop” of the manifolds can grow up and, eventually, can allow the trajectories to escape. At the same time that the point becomes complex unstable, there is a family of invariant curves that detach from the origin.

¹letting aside the possible existence of Arnol'd diffusion.

If we want to compare with the standard (and dissipative) Hopf bifurcation in dimension two, this corresponds to the case in which there is an elliptic periodic orbit that detaches from the origin at the same time that the origin becomes unstable. Note that, although the origin is unstable, the dynamics close to it is still “trapped” by the small periodic orbit. In the next sections we will illustrate this in detail.

3.1 The Lyapunov families of invariant curves

We will first consider values of $L < L_{crit} = \frac{1}{4}$. In this case, the eigenvalues of the Jacobian matrix A are given by $\lambda = \exp(\pm i\omega_1)$, $\mu = \exp(\pm i\omega_2)$, and the linear dynamics around the fixed point is described by the product of two harmonic oscillators. Under generic conditions, it can be proved that each linear oscillation gives rise to a Cantorian 1-parametric family of invariant curves with a rotation number that tends to ω_i , $i = 1, 2$ when the invariant curves tend to the fixed point (see [JV97a], [JV98], [JV01]). The parametrisation of these families is only defined on a set of values of the parameter of positive Lebesgue measure and empty interior. It is remarkable that, if the frequencies of the linearization around the origin are Diophantine and the map is analytic, the size of the holes that conform the Cantor structure of the families are exponentially small with the distance to the origin. Due to the similarities with the periodic orbits predicted by the well-known Lyapunov’s centre theorem ([MH92]), we refer to these families as Lyapunov families of invariant curves.

The numerical computation of these families has been carried out by the method described in Section 5.1. We note that, although we are computing a Cantorian family of invariant curves, the holes are too small to be seen with the standard double precision arithmetic of the computer. In fact, if the continuation method “falls” in one of the holes, the program fails to compute the curve and stops with the corresponding error message, which has never happened in our computations. In summary, for numerical purposes, we can deal with these families as if they were continuous. As described in Section 5.1, the computation of invariant curves is based on the computation of the Fourier coefficients of a parametrisation of the curve, $x(\theta)$ ($\theta \in \mathbb{T}^1$) such that $T_s(x(\theta)) = x(\theta + \omega)$, being $\omega \in \mathbb{R}$ the rotation number. As this parametrisation is not unique, we add the condition $x_1(0) = 0$ ($x_1(\theta)$ denotes the first component of $x(\theta)$). In what follows, to simplify the notation, we will denote the values $x(0)$ as \tilde{x} , so the previous condition is simply written as $\tilde{x}_1 = 0$.

Figure 1 shows the two Lyapunov families obtained for different values of L ($L = 0.24$, 0.245 and 0.249). The rotation number is on the horizontal axis and the value \tilde{x}_2 is on the vertical one. We plot in Figure 2 an invariant curve obtained for each family when $K = -1$ and $L = 0.24$. As we can see in Figure 1, for each value of L , the corresponding two families of invariant curves have a rotation number that tends to the arguments of the eigenvalues of the elliptic fixed point where the families are born (the values ω_i , $i = 1, 2$, see also Table 1). On the other hand, when L tends to L_{crit} , the values ω_i , $i = 1, 2$, get closer and tend to a value ω_{crit} such that $\alpha = -4 \cos(\omega_{crit}) = -(4 + K)$ (in this example $\omega_{crit} = \arccos(3/4) \approx 0.72273424781342$).

It is also known that, near the fixed point, these invariant curves have the same normal

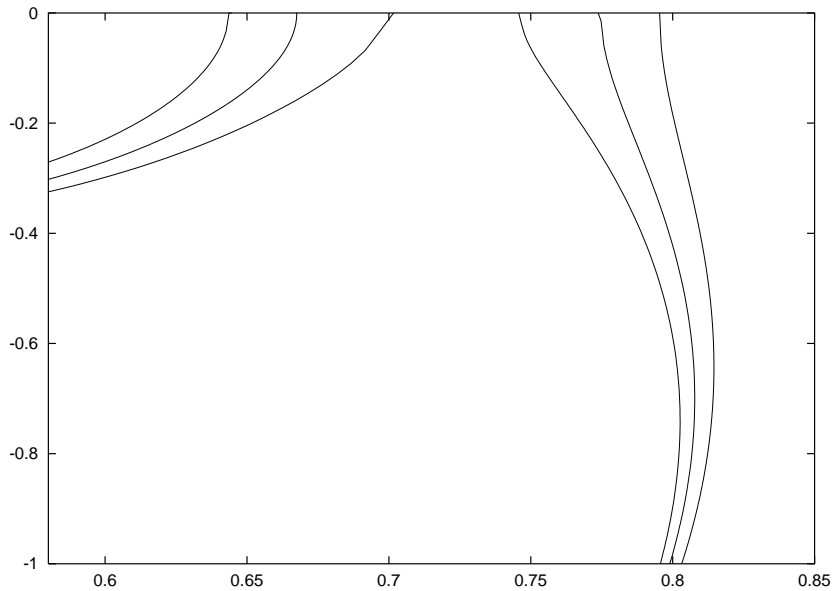


Figure 1: Lyapunov families of invariant curves (rotation number ω versus \tilde{x}_2) of the mapping T_s , for different values of $L < L_{crit}$: we plot both families (from the outer to the inner ones) for $L = 0.24, 0.245$ and 0.249 .

L	ω	
0.24	0.64350110879329	0.79539883018414
0.245	0.66752639710877	0.77468035122454
0.249	0.69849419144132	0.74632549050620
0.25	0.72273424781342	0.72273424781342

Table 1: Limit rotation numbers

behaviour as the initial elliptic point.² It is also known ([JV97a], [JV97b] and [JV01]) that the elliptic directions of these curves give rise to a family of 2D invariant tori, in the same way the elliptic directions of the point give rise to families of invariant curves. These families of 2D tori are also obtained from the application of the KAM tori around the elliptic fixed point. The two Lyapunov families of invariant curves can be seen as a kind of skeleton for these 2D tori.

3.2 Complex unstable fixed points. Invariant manifolds

If $L > L_{crit}$, the origin is complex unstable. Then, we can compute its 2D real unstable (stable) invariant manifolds with the method explained in Section 5.3. For instance, let us focus on the case $L = 0.26$. Figure 3 (top, left) shows a curve inside the linearisation

²With the exception of curves that are in a suitable resonance between the normal and internal frequencies (see [BHJ⁺02] for more details about this phenomenon). These “resonant” curves have very small measure and they are “below computer resolution” in the examples shown here.

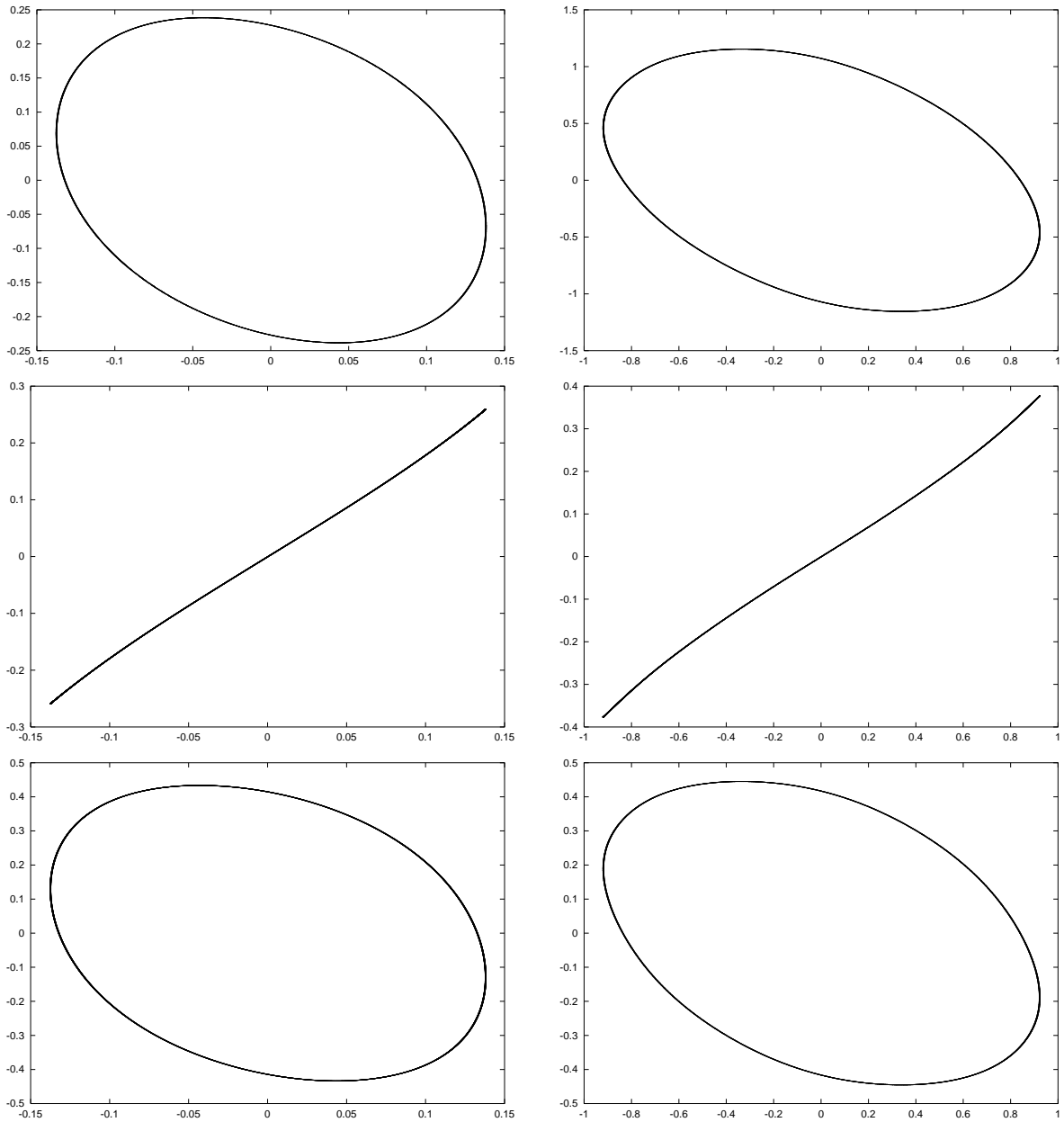


Figure 2: Two particular invariant curves for the mapping T_s , with $L = 0.24$. Left column: (x_1, x_2) , (x_1, x_3) and (x_1, x_4) projections of the curve with $\tilde{x}_2 = -0.22729180238$ and $\omega = 0.6008342478$. Right column: (x_1, x_2) , (x_1, x_3) and (x_1, x_4) projections of the curve with $\tilde{x}_2 = -1.0712574172$ and $\omega = 0.798309349426$.

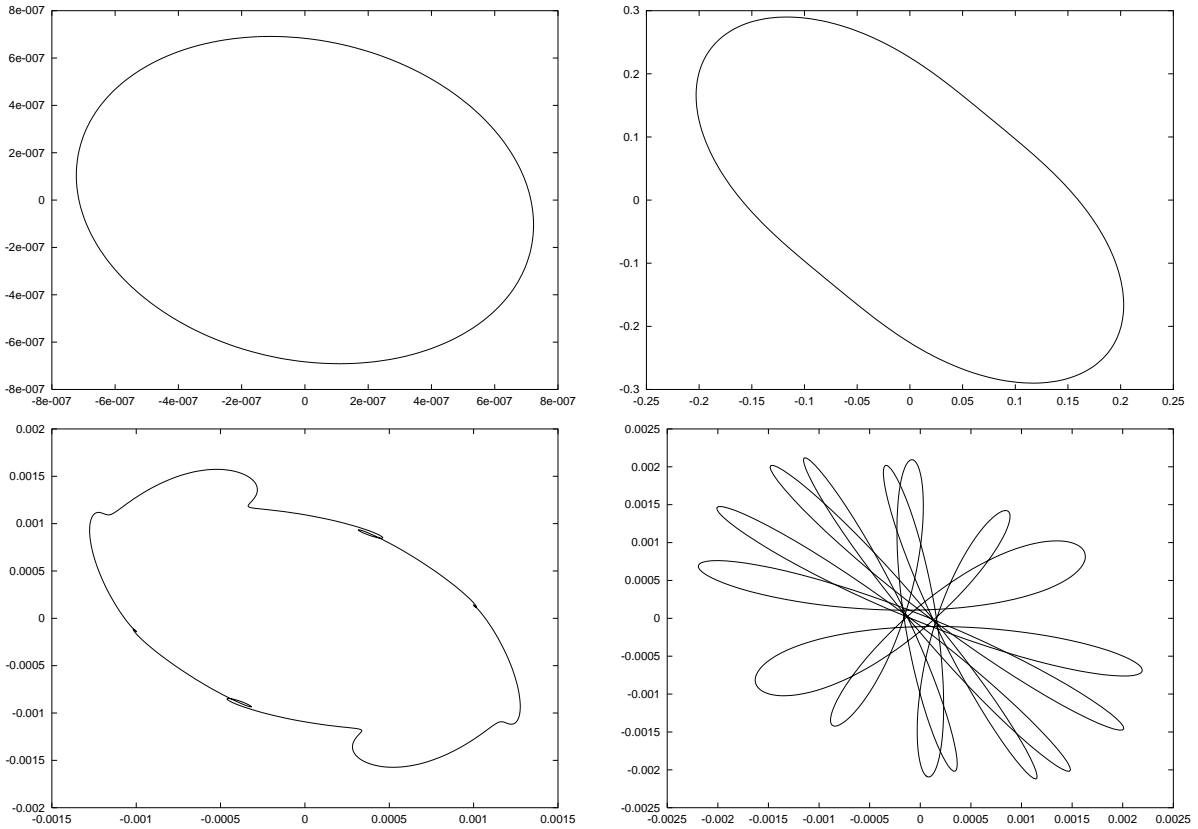


Figure 3: Mapping T_s , $L = 0.26$. (x_1, x_2) projection of the k -iterate of an initial curve on the unstable manifold of the origin. Top left: $k = 1$, right: $k = 200$, bottom left: $k = 270$, right: $k = 300$.

at $x = 0$ of the unstable manifold. This curve is close enough to the origin so that the error of the linear approximation is below 10^{-12} (this is the curve called σ in Section 5.3). If we compute 200 (270 and 300) iterates of the curve, we obtain the whole Figure 3.

The same kind of computation can be done for the stable manifold, using the suitable eigenvectors and mapping T_s^{-1} (see Figure 4). We remark the intricate behaviour of the iterates on the invariant manifolds; we can see in Figures 3 and 4 how the iterates go far away (see the different size of the windows in both figures) and then back very close to the origin in a chaotic way. The increasing complexity of the iterates in Figures 3 and 4 is due to the lack of coincidence of the stable and unstable manifolds: they must coincide for an integrable Hamiltonian system (in a similar way as described in [Mee85] and [Mey98] in a two degree of freedom context), but they are almost coincident for nearly integrable systems and the phenomenon of splitting of separatrices appears.

It is also interesting to look at slices of these manifolds, to get a better understanding of their behaviour. For instance, for the case $L = 0.26$ we have cut the manifolds with the hyperplane $x_1 = 0$, see Figure 5 (top) for the unstable manifold and Figure 5 (bottom) for the stable one. The manifolds seem to coincide because, close to the origin, the system is close to an integrable one. As the parameter L grows, so do the invariant manifolds and

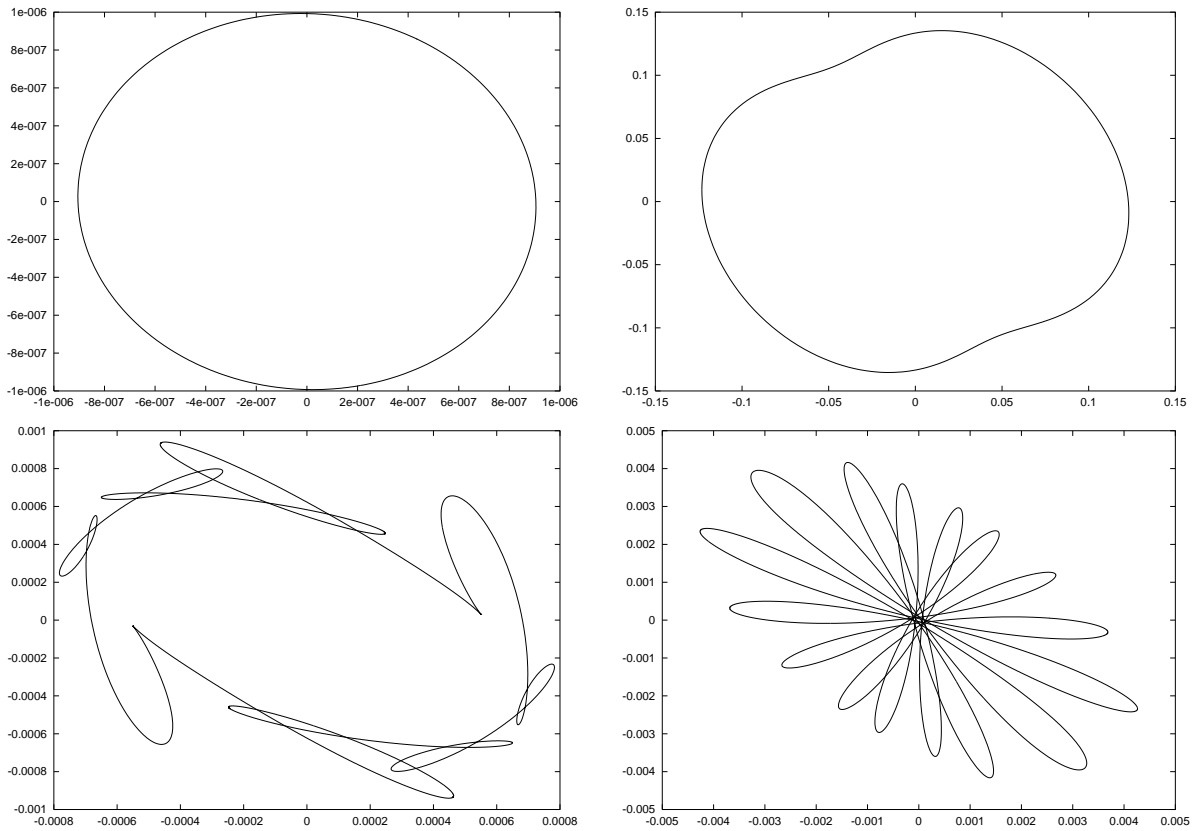


Figure 4: This is the same plot as Figure 3 but for the stable manifold.

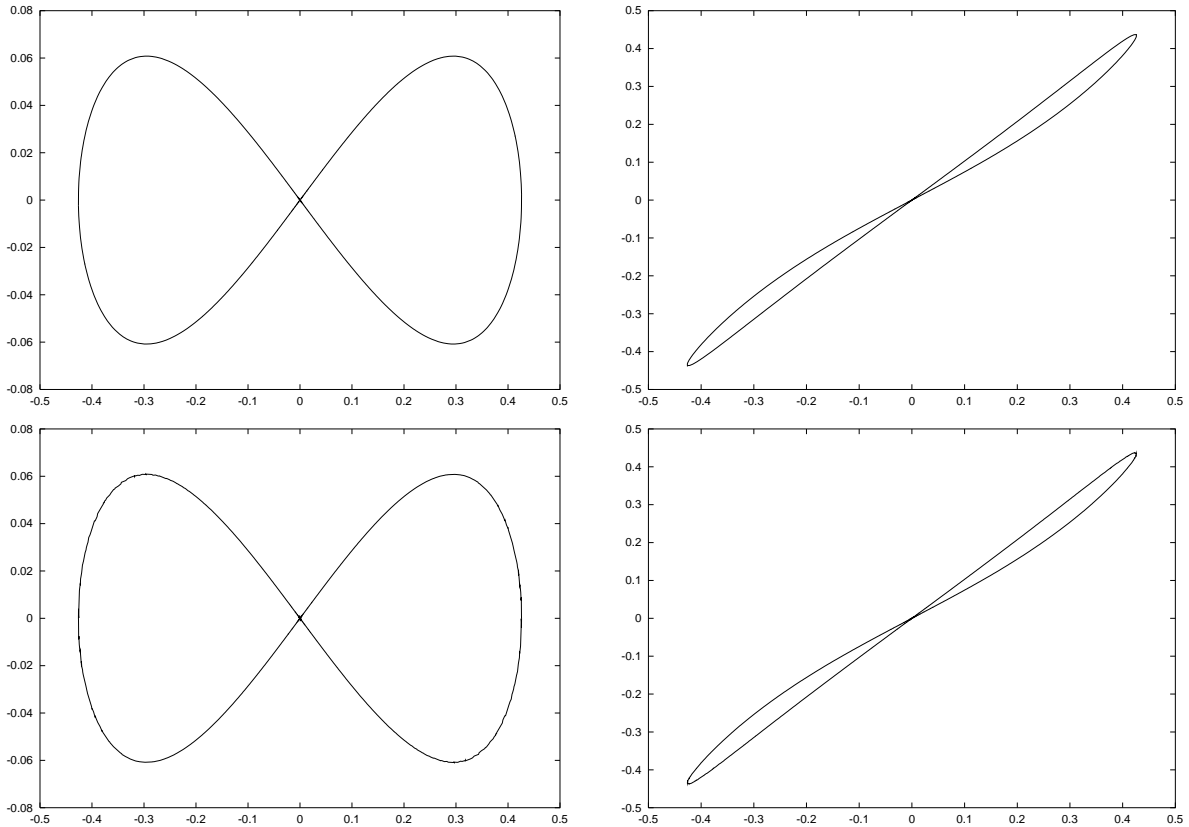


Figure 5: Mapping T_s , $L = 0.26$. Intersection between the invariant manifold and $x_1 = 0$. Top: W^u , (x_2, x_3) and (x_2, x_4) projections; bottom: W^s .

they are not almost coincident anymore: we can see in Figure 6 the slice of the unstable and stable manifolds for T_s , and increasing values of L ($L = 0.28$ and $L = 0.3$). On the contrary, when L decreases to L_{crit} the invariant manifolds shrink to the origin.

3.3 Unfolding of tori. Hopf bifurcation

We note that the analytical techniques used in [OPV] imply the phenomenon observed in Figure 7, where we show the Lyapunov families of invariant curves for several values of L . Let us explain this figure in detail. In the vertical axis, we show the value of the x_2 coordinate of the curve when $x_1 = 0$, while the horizontal axis is the rotation number. If we look at $x_2 = 0$ (the top axis of the plot), we see that there are several curves departing from it (they are, in fact, departing from the origin), that correspond to the values $L = 0.24$, $L = 0.245$, $L = 0.249$ and $L = L_{crit} = 0.25$ (the linear frequencies at the origin are given in Table 1). We have also included the continuation of these families for $L = 0.26$, $L = 0.27$, $L = 0.29$ and $L = 0.31$: they appear as a single curve that moves down in the graphic as L increases.

So, Figure 7 shows how the two families of Lyapunov invariant curves that exist for $L < L_{crit}$ and that are born at the origin, meet at $L = L_{crit}$ and detach from $x = 0$ as a

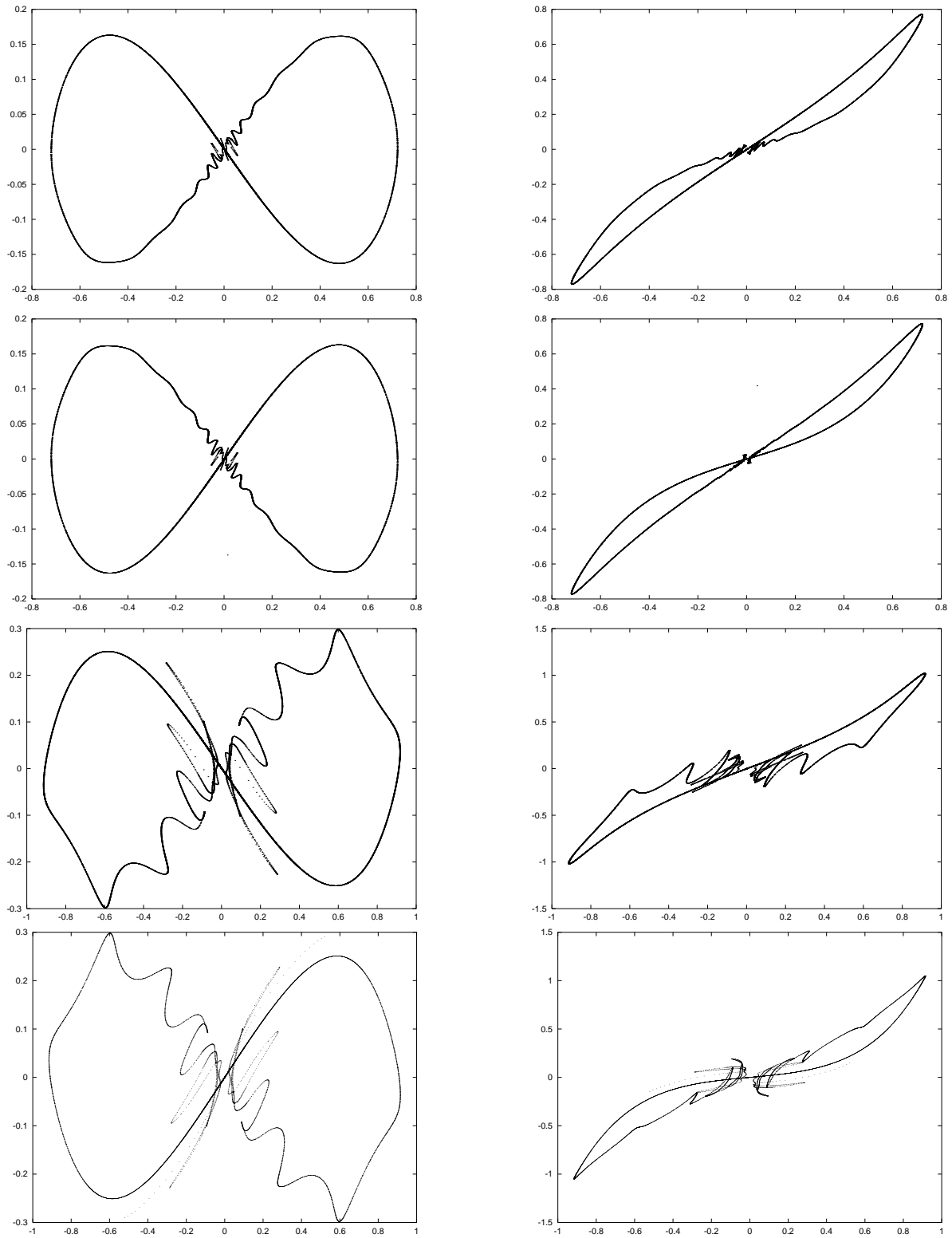


Figure 6: Mapping T_s . Intersection between the invariant manifold and $x_1 = 0$. First row: $L = 0.28$, W^u , (x_2, x_3) and (x_2, x_4) projections; second row: $L = 0.28$, W^s , third row: $L = 0.30$, W^u and last row: $L = 0.30$, W^s .

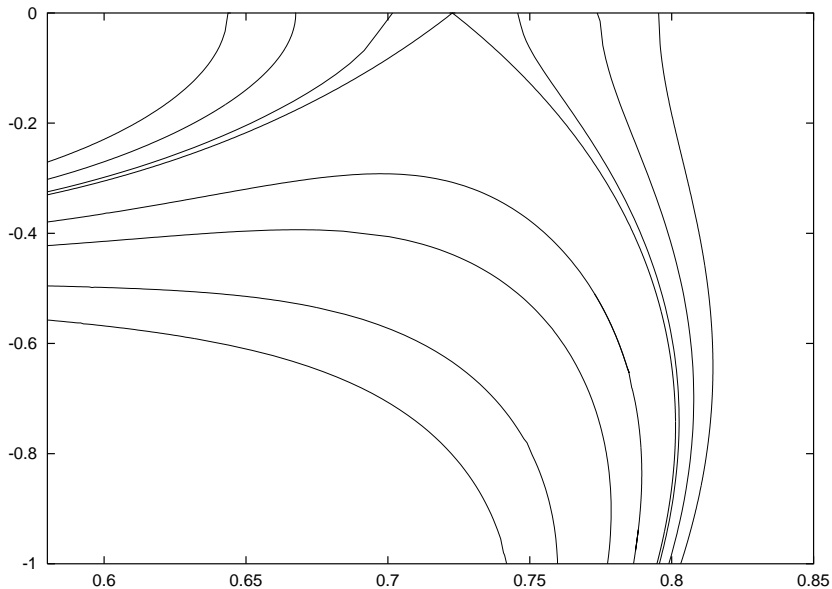


Figure 7: Detachment of the Lyapunov families of invariant curves of the mapping T_s (rotation number ω versus \tilde{x}_2), when L crosses L_{crit} . See the text for more details.

unique family for $L > L_{crit}$. That is, for a fixed $L > L_{crit}$, the origin is complex unstable, but there is a family of invariant curves at some finite distance from the origin.

This bifurcation is analogous to the classical direct Hamiltonian Hopf bifurcation in Hamiltonian vector fields (see [Mee85] and references therein) when, along a family of equilibrium points, two pairs of pure imaginary eigenvalues collide on the imaginary axis and become a complex quadruplet outside the imaginary axis, and a family of stable periodic orbits is detached from the two Lyapunov families that exist before the collision. Here, the Lyapunov families of invariant curves keep their elliptic character when they detach from the origin at the transition to complex instability. Using the techniques described in Section 5.2, we can compute the linear normal eigenvalues of a given invariant curve. Due to the symplectic character of the mappings, an elliptic invariant curve will have 1 (twice), $\lambda = \exp(i\nu)$ and $\bar{\lambda} = \exp(-i\nu)$ as normal eigenvalues. For example, we show in Figure 8 the argument ν of some families of invariant curves computed for $L = 0.24$ (the higher and lower curves), 0.25 (the two curves that meet at $x = 0$) and 0.27 (the single curve that keeps away from $x = 0$). The holes that conform the Cantor structure of these invariant curves are too small to be seen at this scale. It is known ([JV97b]) that normally elliptic invariant curves are surrounded by maximal dimensional tori, so this shows the coexistence of 2D tori with the invariant manifolds of the origin for values of L larger than L_{crit} .

3.4 Confinement. Invariant curves and 2D tori

A natural question that arises is to describe the dynamics close to the origin before and after the transition to complex instability. On one hand, we show in Figure 9 the evolution

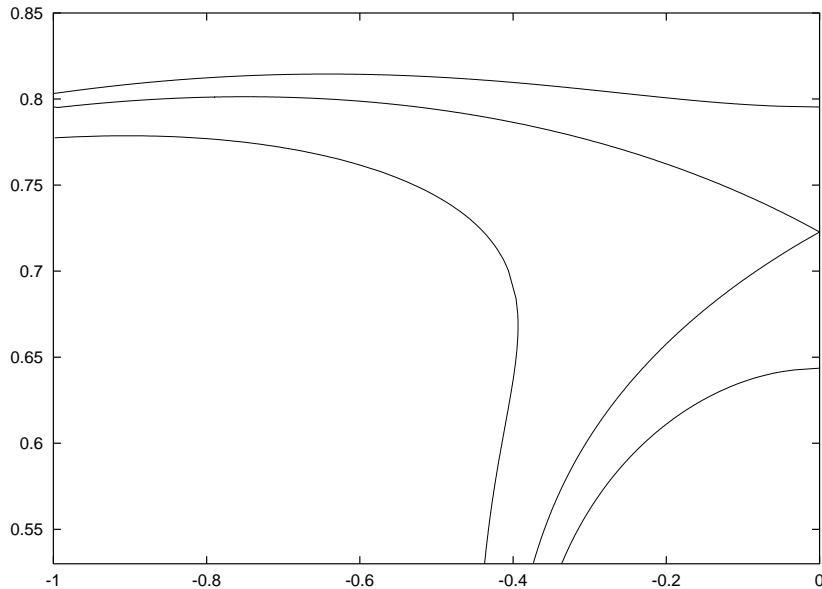


Figure 8: Mapping T_s , horizontal axis: \tilde{x}_2 , vertical one: argument of the normal eigenvalue of the invariant curves of the families obtained for $L = 0.24, 0.25$ and 0.27 .

of a KAM (2D) torus before, at and after the transition: for T_s , $K = -1$, $L = 0.249$ (top row), $L = 0.25$ (middle row) and $L = 0.251$ (bottom row), we plot the iterates of the initial condition $x_i = 0.001$, $i = 1, \dots, 4$; we note how the size of the plot increases after the transition due to the existence of the invariant manifolds and the iterates are close to the invariant manifolds associated to the unstable origin and therefore follow their shape. Of course, the iterates on a 2D torus remain confined forever, however, the phenomenon of Arnol'd diffusion may appear; for this mapping Nekhoroshev's estimates of diffusion were given in [OP99b]. It is worth remarking the (x_1, x_3) projection in Figure 9 (middle column); as stated in [Pfe85a] and Section 2, the set of tori at $\Delta = 0$ ($L = L_{crit}$) collapses onto a plane.

In Figure 10 we show the effect of the bifurcation on the topology of the 2D tori in a region close to the origin. We consider T_s , $K = -1$ and we take as initial conditions $x_1 = x_2 = x_3 = x_4$, for different values of x_1 , that is, 0.1, 0.07 and 0.001; we can see the evolution, when varying L , of the 2D tori (their slices in the figure) as well as the influence of the invariant manifolds of the complex unstable origin, for $L > L_{crit}$. Finally, we also remark that the invariant curves and the 2D tori coexist with the invariant manifolds (which do not separate any region in the (x_1, x_2, x_3, x_4) space).

4 Inverse bifurcation

Corresponds to the map T_t . As before, we will select $K = -1$. First, let us briefly describe this bifurcation. For $L < L_{crit}$, the origin is surrounded by 2D invariant tori. When L approaches L_{crit} , there is a set of hyperbolic invariant curves that approaches the origin and the region filled by the maximal dimensional tori shrinks to the origin. When L

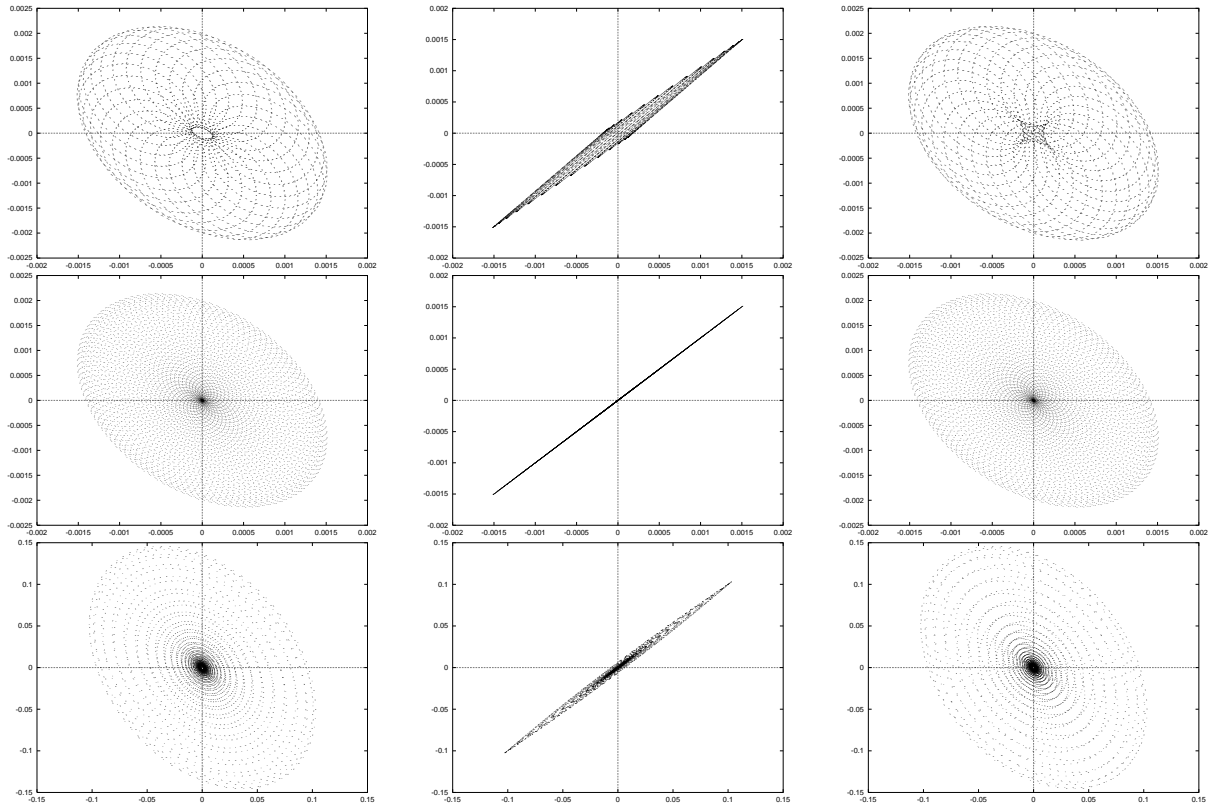


Figure 9: Mapping T_s . (x_1, x_2) , (x_1, x_3) and (x_1, x_4) projections of a 2D torus before the transition ($L = 0.249$, top), at the transition ($L = 0.25$, middle) and after it ($L = 0.251$, bottom). We note the different scale for the frame in each case.

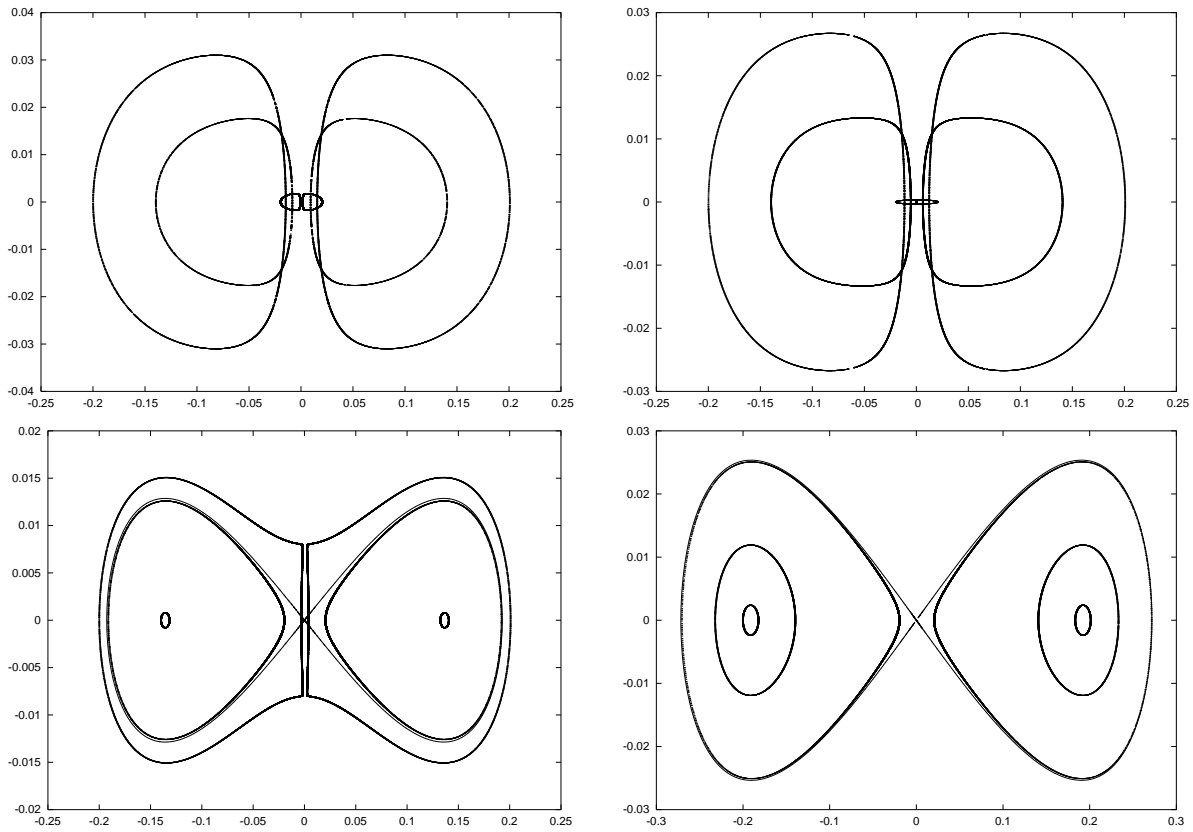


Figure 10: Mapping T_s . (x_2, x_3) projection of the slice $x_1 = 0$ of different 2D tori obtained from the same initial conditions but with different L . Top left: $L = 0.249$, top right: $L = 0.25$, bottom left: $L = 0.252$ and bottom right: $L = 0.254$. For $L > 0.25$ we also plot the slices of the invariant manifolds.

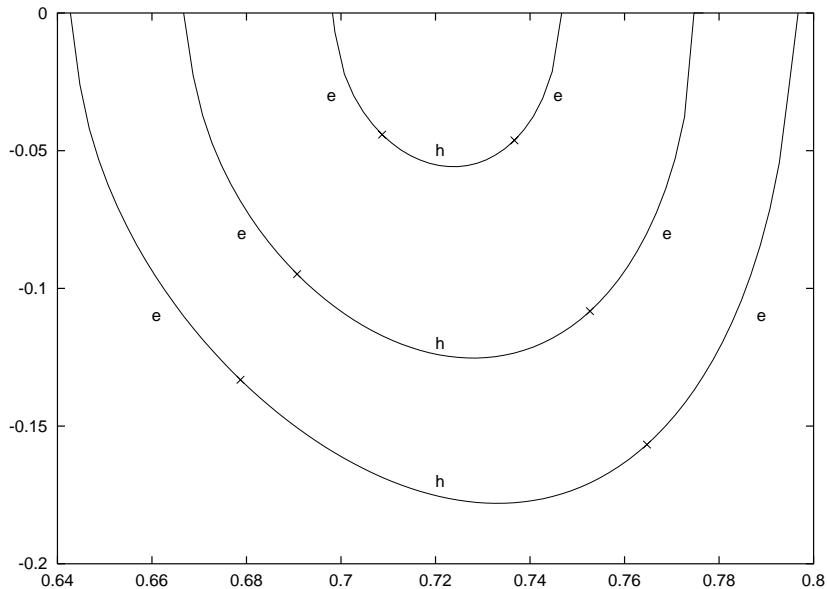


Figure 11: Mapping T_t . The global family of invariant curves for $L = 0.24$, $L = 0.245$ and $L = 0.249$ (outer to inner ones); rotation number versus \tilde{x}_2 . The marked points correspond to transition invariant curves.

crosses L_{crit} , the origin becomes hyperbolic and its stable and unstable manifolds are not necessarily connected (compare with the direct case). Hence, all the nearby trajectories escape (except, of course, the ones on the stable manifold).

We can compare with the classical 2D (and dissipative) Hopf bifurcation. This corresponds to the case in which there is an unstable periodic orbit that approaches to the (stable) origin. Then, the orbit merges the fixed point that becomes unstable too. This means that the dynamics after the bifurcation is “trivial”, in the sense that all the trajectories escape. In the following sections we will show this in more detail.

4.1 The Lyapunov families of invariant curves

As before, for $L < L_{crit}$, we compute the two Lyapunov families of invariant curves that are born at the origin. The continuation process shows that these two families meet at some distance from the origin. In other words, for each $L < L_{crit}$ we have one global family which begins and ends at the origin. When L approaches L_{crit} , this “connecting loop” collapses to the origin. This is illustrated in Figure 11, where these families are computed for $L = 0.24$, 0.245 and 0.249 .

Concerning the stability of each global family, it is as follows: near the origin, the invariant curves are mostly³ elliptic (they have been marked with an “e” in Figure 11), as expected due to the stable character of the origin. At some distance of $x = 0$, they become hyperbolic (marked with an “h” in Figure 11). Therefore, each family has two parabolic (transition) invariant curves (also marked in Figure 11). The numerical methods used

³Except by a set of very small measure, see [BJH⁺02].

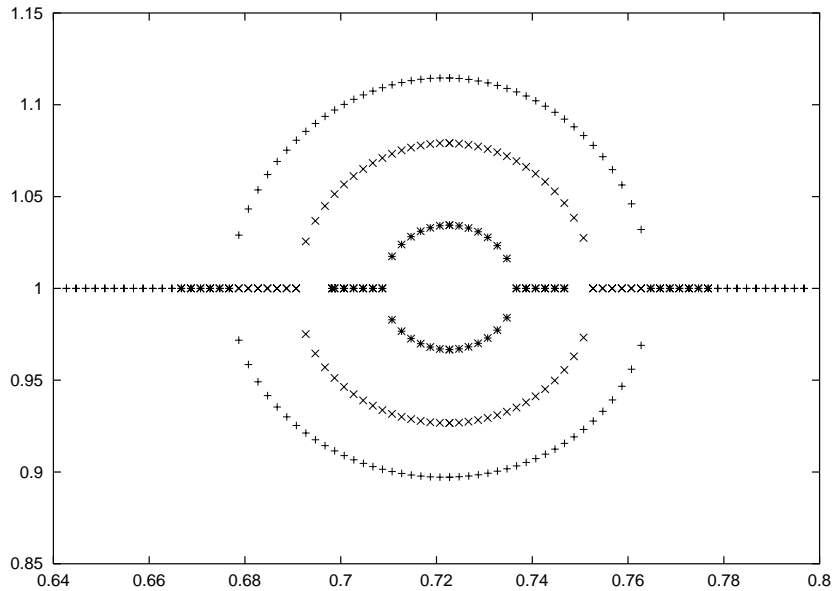


Figure 12: Mapping T_t . Normal behaviour of the invariant curves: rotation number versus the modulus of the normal eigenvalues.

for the computation of the normal eigenvalues (Floquet reduction) of the curves have been summarised in Section 5.2. In Figure 12, for several values of L (0.24, 0.245 and 0.249), we plot the rotation number versus the modulus of the normal eigenvalues. For elliptic invariant curves, the eigenvalues are in the unit circle (modulus one) whereas for hyperbolic ones, there are two (real) eigenvalues with modulus different from 1 (with product equal to 1). This shows the hyperbolic character of the invariant curves that are at some distance from the origin.

4.2 Invariant manifolds

We have computed the stable and unstable manifolds of the hyperbolic invariant curves of the previous section (for more details about this computation, see Section 5.3.2). Figure 13 (top, left) shows the (x_2, x_3) projection of the slice $x_1 = 0$ of the invariant manifolds of one of the hyperbolic invariant curves, for $L = 0.24$. These manifolds are “nearly connected” in one side of the curve, while in the other side they are far from being connected. As the invariant curve cuts $x_1 = 0$ in two points, the manifolds appear twice in the plots. Figure 13 (top, right) corresponds to $L = 0.249$. Note that the invariant curve gets closer to the origin and the stable and unstable manifolds that are nearly connected tend to collapse to the origin as well. When L reaches the critical value $L_{crit} = 0.25$, the hyperbolic curves and their nearly connected manifolds merges with the origin so that it becomes a parabolic point. The existence of parabolic invariant manifolds for $L = L_{crit}$ follows from the resonant normal form (for an explicit expression of this normal form see [Pac02]). If $L > L_{crit}$, the invariant curves have disappeared and the origin is complex unstable; its invariant manifolds are shown in Figure 13 (bottom, left) and (bottom, right)

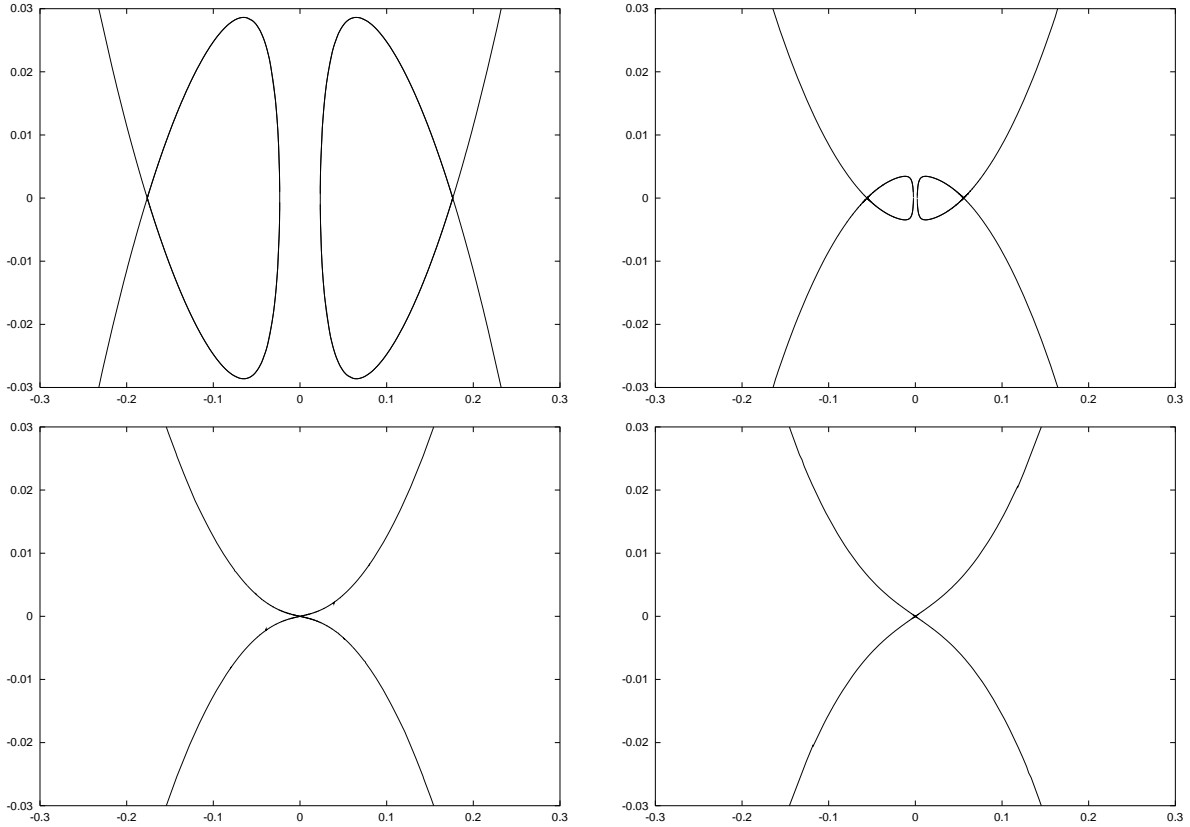


Figure 13: Mapping T_t . These plots show the (x_2, x_3) projections for the slice $x_1 = 0$ of the stable and unstable invariant manifolds of an invariant curve (top plots) and the origin (bottom plots), when the invariant curve collapses at $x = 0$. Top left: $L = 0.24$; top right: $L = 0.249$; bottom left: $L = 0.2501$; bottom right: $L = 0.251$. See the text for details.

for $L = 0.2501$ and $L = 0.251$ respectively.

As analysed in [Mey98] (for equilibrium points) and [Pac02] (for periodic orbits), the stable and unstable 2D invariant manifolds that develop from an equilibrium undergoing an inverse transition to complex instability are rather far from being connected. This is also what happens here (see Figure 13, bottom). For $L > L_{crit}$ the iterates of any point close to the origin go away quite fast, as expected.

5 Summary of numerical methods

This section summarises the main numerical techniques used. To fix the notation, let us assume that we are dealing with an autonomous discrete dynamical system defined by

$$\bar{x} = f(x), \quad (3)$$

for x in some domain of \mathbb{R}^n . In what follows, we will assume that the length of \mathbb{T}^1 is 2π .

5.1 Invariant curves

Assume that (3) has an (at least continuous) invariant curve, whose parametrisation is denoted by $\theta \in \mathbb{T}^1 \mapsto x(\theta) \in \mathbb{R}^n$, that is,

$$f(x(\theta)) = x(\theta + \omega),$$

where the rotation number ω is assumed to be known and irrational, $\omega \notin 2\pi\mathbb{Q}$. Let $C(\mathbb{T}^1, \mathbb{R}^n)$ be the space of continuous functions from \mathbb{T}^1 in \mathbb{R}^n , and let us define the linear map $T_\omega : C(\mathbb{T}^1, \mathbb{R}^n) \rightarrow C(\mathbb{T}^1, \mathbb{R}^n)$ as the translation by ω , $(T_\omega x)(\theta) = x(\theta + \omega)$. Then, let us define $F : C(\mathbb{T}^1, \mathbb{R}^n) \rightarrow C(\mathbb{T}^1, \mathbb{R}^n)$ as

$$F(x)(\theta) = f(x(\theta)) - T_\omega(x(\theta)), \quad \forall x \in C(\mathbb{T}^1, \mathbb{R}^n).$$

It is clear that the zeros of F correspond to (continuous) invariant curves of (3) with rotation number ω . The method summarised here boils down to look numerically for these zeros. To this end, let us write $x(\theta)$ as a real Fourier series,

$$x(\theta) = a_0 + \sum_{k>0} a_k \cos(k\theta) + b_k \sin(k\theta), \quad a_k, b_k \in \mathbb{R}^n, \quad k \in \mathbb{N}.$$

Then, we will fix in advance a truncation value N for this series (the selection of N will be discussed later on), and let us try to determine (an approximation to) the $2N + 1$ unknown coefficients a_0 , a_k and b_k , $1 \leq k \leq N$. To this end, we will construct a discretized version of the map F , as follows: first, we take the mesh of $2N + 1$ points on \mathbb{T}^1 ,

$$\theta_j = \frac{2\pi j}{2N + 1}, \quad 0 \leq j \leq 2N.$$

So, given a (known) set of Fourier coefficients a_0 , a_k and b_k ($1 \leq k \leq N$), we can compute the points $x(\theta_j)$, then $f(x(\theta_j))$ and next the points $f(x(\theta_j)) - x(\theta_j + \omega)$, $0 \leq j \leq 2N$. From this data, it is immediate to obtain the Fourier coefficients of $f(x(\theta)) - x(\theta + \omega)$. Let us call F_N to this discretization of F . Note that if we only want to solve the equation $F_N = 0$, the last step in the evaluation of F_N (the obtention of the Fourier coefficients) can be avoided, since this is an invertible linear operator –so it maps 0 to 0– that does not affect to the solutions of $F_N = 0$; this is what has been done in [Jor00], [CJ00] and [Oll00].

To apply a Newton method to solve the equation $F_N = 0$, we also need to compute explicitly the differential of F_N . This can be done easily by applying the chain rule to the process used to compute F_N .

With the previous definitions, it is clear that if $x(\theta)$ is a Fourier series corresponding to an invariant curve then, for any $\varphi \in \mathbb{T}^1$, $y(\theta) \equiv x(\theta + \varphi)$ is a different Fourier series (i.e., the Fourier coefficients are different) corresponding to the same invariant curve as $x(\theta)$. This implies that the differential of the function F around an invariant curve will have, at least, a one-dimensional kernel. This introduces numerical difficulties when solving the linear system that appears in the Newton method. To solve this problem we simply add, for instance, an extra condition imposing that a component of $x(\theta)$ has a prescribed value when θ is zero (of course, there are different options). On one hand, this removes

the lack of uniqueness problem and, on the other hand, this can be imposed in a very easy way: we simply add this condition as an extra equation and, as this is a linear condition, we simply add the corresponding row in the Jacobian of F . Note that now we have to solve a linear system that has a unique solution, but it is not “squared”: it has an “extra” equation. If, for instance, we are solving the linear system by means of a standard Gaussian elimination method with row pivoting, then the pivoting strategy will take care of sending to the last row the equation that is linearly dependent of the other equations. So, after the triangularisation process and except by rounding errors, the last equation should read like “ $0 = 0$ ”. Hence, we can simply skip this equation and solve the triangular system in the usual way.

To select the truncation value N used in the discretization of the operator L_ω , we will use the following estimation for the error:

$$E(x, \omega) = \sup_{\theta \in \mathbb{T}^1} |f(x(\theta)) - x(\theta + \omega)|.$$

Clearly, x is an invariant curve with rotation number ω iff $E(x, \omega)$ is zero. Then, for each curve, we have estimated the quantity $E(x, \omega)$ by simply tabulating its value on a mesh of points on \mathbb{T}^1 . Of course, this mesh must be finer than the one used in the discretization of L_ω . When this estimate is bigger than a prescribed threshold (here we have used 10^{-12}), the program automatically increases the truncation value N and recomputes the invariant curve. This process is repeated until the estimated error $E(x, \omega)$ is lower than 10^{-12} .

The continuation of families of curves follows the same rules as the continuation of fixed points and periodic orbits. We refer to [CJ00] for a more detailed discussion for the case of invariant curves. There you will also find a discussion about how to choose a first guessing for the frequency to start the continuation.

5.2 Linear normal behaviour around invariant curves

As before, let $\theta \in \mathbb{T}^1 \mapsto x(\theta) \in \mathbb{R}^n$ denote an invariant curve of a map f . Then, its linearised normal behaviour is described by the linear dynamical system

$$\left. \begin{aligned} \bar{x} &= A(\theta)x \\ \bar{\theta} &= \theta + \omega \end{aligned} \right\}, \quad (4)$$

where $A(\theta) = D_x f(x(\theta))$. This kind of system is sometimes known as linear quasi-periodic skew-product.

The system (4) is called reducible iff there exists a (may be complex) change of variables $x = C(\theta)y$, $\theta \in \mathbb{T}^1$, such that (4) becomes

$$\left. \begin{aligned} \bar{y} &= By \\ \bar{\theta} &= \theta + \omega \end{aligned} \right\}, \quad (5)$$

where the matrix $B \equiv C^{-1}(\theta + \omega)A(\theta)C(\theta)$ does not depend on θ .

In what follows, $C(\mathbb{T}^1, \mathbb{C}^n)$ will denote the space of continuous functions from \mathbb{T}^1 to \mathbb{C}^n , endowed with the sup norm. We denote by L_ω the linear operator of $C(\mathbb{T}^1, \mathbb{C}^n)$ defined

as $L_\omega\psi = [T_{-\omega} \circ A]\psi$, that is,

$$(L_\omega\psi)(\theta) = A(\theta - \omega)\psi(\theta - \omega).$$

The reducibility of (4) can be characterised in terms of the spectrum of L_ω . The details can be found in [Jor01], and here we will simply summarise the most relevant results.

Proposition 5.1 *Let $\lambda \in \mathbb{C}$ be an eigenvalue of L_ω . Then, for any $k \in \mathbb{Z}$, $\lambda \exp(i k \omega)$ is also an eigenvalue of L_ω .*

Definition 5.1 *Two eigenvalues λ_1 and λ_2 are said to be ω -unrelated iff $\lambda_1 \neq \lambda_2 \exp(i k \omega)$ for all $k \in \mathbb{Z}$.*

Proposition 5.2 *Assume that there exists n ω -unrelated eigenvalues $\lambda_1, \dots, \lambda_n$ for L_ω . Then, (4) can be reduced to (5), where $B = \text{diag}(\lambda_1, \dots, \lambda_n)$. Moreover, if the spectrum of L_ω is larger than the closure of the set of eigenvalues, then (4) cannot be reduced to constant coefficients.*

These results imply that a possibility to study the reducibility of (4) is to approximate numerically the spectrum of L_ω . This is the approach we have followed in this paper.

The computations are based on the same discretization used in Section 5.1 to compute invariant curves. This is, given a truncation value N , it is not difficult to derive the matrix (of dimension $n(2N + 1)$) corresponding to the discretization of the operators $\psi(\theta) \mapsto A(\theta)\psi(\theta)$ and $T_{-\omega}$. Then, the product of these two matrices gives the truncation of L_ω . Finally, the spectrum is approximated by a shifted QR iteration.

It is possible to derive estimates on the truncation error of the eigenfunctions from the decay of their Fourier coefficients and their size at the truncation point. Therefore, it is also possible to select, among the computed eigenfunctions, the most accurate ones –and, hence, the most accurate representants of the classes of ω -related eigenvalues– for the actual truncation. It turns out that all the invariant curves that appear in this paper are reducible, at least within an accuracy of 10^{-12} .

We refer to [Jor01] for a more complete description of these ideas and procedures.

5.3 Invariant manifolds

The approximation of invariant manifolds is a standard computation in applied dynamical systems (see, for instance, [GJMS93], [Sim94], [KO98]). Due to the particularities of our cases, we have used specific methods that we explain in this section. In particular, from now on, the map f in (3) will be 4D.

5.3.1 Manifolds of a complex unstable fixed point

Assume that the origin is a fixed point of f , with eigenvalues of the form $r_{1,2} \exp(\pm i \omega)$, $0 < r_1 < 1$, $r_2 > 1$ and $\omega \notin \pi\mathbb{Z}$. Let us start discussing the computation of the unstable manifold. Therefore, we select the eigenvalue $r_2 \exp(i \omega)$ and we denote by $u + i v$ (u and v are unitary vectors in \mathbb{R}^4) the corresponding eigenvector. Then, the vectors u and v span

the linear approximation to the (2D) unstable manifold, that is a good approximation to the real manifold in a small neighbourhood of the point. In order to follow the manifold outside this small neighbourhood, we consider the closed curve on the linear approximation to the manifold defined by

$$\sigma(s) = h \frac{\tilde{\sigma}(s)}{\|\tilde{\sigma}(s)\|}, \quad \text{where } \tilde{\sigma}(s) = \cos(s) \cdot u + \sin(s) \cdot v, \quad s \in [0, 2\pi], \quad (6)$$

where h is a small quantity. In order to check the smallness of h to guarantee that the tangent plane is a good enough approximation of the unstable invariant manifold, we carry out the following test: given $a = \alpha u + \beta v$, $\alpha, \beta \in \mathbb{R}$, with $\|a\| = 1$, we have

$$T_i(ha) = h [(\alpha a + \beta b)u + (\beta a - \alpha b)v] + O(h^2), \quad i \in \{s, t\},$$

The difference (the term $O(h^2)$) can be computed explicitly and measures how far is the value $T_i(ha)$ from the plane generated by u and v . We have done such computation considering as a the points in the curve $\sigma(s)$, $s \in [0, 2\pi]$, and it turns out that, in our examples, if $h \leq 10^{-5}$ the term $O(h^2)$ is less than 10^{-15} . Then, we can use these values as starting points for trajectories on the unstable manifold.

A first approach to compute the iterates of the curve σ defined before is to simply take a uniformly spaced mesh on the curve and to compute the images of these points under f . The main inconvenience is that the mesh can loose its uniformity so that the points can accumulate on certain parts of the curve. To avoid that, we proceed as follows. If we denote by $\{p_j\}_j$ the initial points on σ , we first compute the points $\{f(p_j)\}_j$ and then we apply a Fourier transform to obtain the Fourier coefficients of (an approximation to) $f \circ \sigma$. Finally, we re-mesh this new curve so that the new points are equispaced according to the arc parameter on the curve. Now, we can restart the process using as $\{p_j\}_j$ the points of this new mesh.

We can apply this procedure to a suitable set of values of h between h_0 and $r_2 h_0$, for a small enough value of h_0 . This produces a set of curves that covers a “fundamental interval” of the manifold.

As we have the Fourier coefficients of each iteration of the curves, it is not difficult to compute their intersection with a given plane. This is what we have done in Sections 3.2 and 4.2 to “slice” the manifolds by a coordinate hyperplane.

Finally, to ensure the correctness of the computations shown here, we have repeated them with quadruple precision (and with different values of h) with no visible differences.

Of course, the same procedure can be used to compute the stable manifold by using the inverse map f^{-1} . In our case this is very easy since we have a closed form for the inverse of the maps considered.

5.3.2 Manifolds of an invariant curve

Let $x(\theta)$ denote an invariant curve of (3), with an irrational rotation number ω . Assume that the linear dynamics around the curve is reducible, and that the reduced matrix has the eigenvalues 1 (twice), λ and λ^{-1} , $\lambda \in \mathbb{R}$, $\lambda > 1$. Let $\psi(\theta)$ be the eigenfunction of L_ω (see Section 5.2) of eigenvalue λ . Then, the linear approximation to the 2D unstable manifold

can be parametrised as $x(\theta) \pm h\psi(\theta)$, where θ and h are the parameters. Now, we are in the same situation as in the previous section, where we used the linear approximation (6) to “grow” the manifold. Note that, in the two cases, we are growing a 2D unstable manifold from a 2D linear approximation in a 4D phase space, so that the other directions are “harmless” (they are either neutral or attractive).

Therefore, we proceed using the same ideas and methods as in the previous section.

Acknowledgements

This research has been supported by the Spanish CICYT grant BFM2000–0623 and the Catalan CIRIT grant 2001SGR–70. À. Jorba acknowledges support from DURSI, and M. Ollé thanks J.R. Pacha and J. Villanueva for interesting discussions and comments.

References

- [BCM95] T.J. Bridges, R.H. Cushman, and R.S. Mackay. Dynamics near an irrational collision of eigenvalues for symplectic mappings. *Fields Inst. Comm.*, 4:61–79, 1995.
- [BHJ⁺02] H.W. Broer, H. Hanßmann, À. Jorba, J. Villanueva, and F.O.O. Wagener. Normal-internal resonances in quasiperiodically forced oscillators: a conservative approach. Preprint, 2002.
- [CB94] G. Contopoulos and B. Barbani. Periodic orbits and their bifurcations in a 3-D system. *Celestial Mech.*, 59:279–300, 1994.
- [CG88] G. Contopoulos and A. Giorgilli. Bifurcations and complex instability in a 4-dimensional symplectic mapping. *Meccanica*, 23:19–28, 1988.
- [CJ00] E. Castellà and À. Jorba. On the vertical families of two-dimensional tori near the triangular points of the Bicircular problem. *Celestial Mech.*, 76(1):35–54, 2000.
- [Fro72] C. Froeschlé. Numerical study of a four-dimensional mapping. *Astron. Astrophys.*, 16:172–189, 1972.
- [GJMS93] G. Gómez, À. Jorba, J. Masdemont, and C. Simó. Study of the transfer from the Earth to a Halo orbit around the equilibrium point L_1 . *Celestial Mech.*, 56:541–562, 1993.
- [Had85] J.D. Hadjidemetriou. The stability of resonant orbits in planetary systems. In *Resonances in the motion of planets, satellites and asteroids*, volume 3 of *Math. Dynam. Astronom. Ser.*, pages 1–18. Univ. São Paulo, São Paulo, 1985.
- [Heg85] D.G. Heggie. Bifurcation at complex instability. *Celestial Mech.*, 35:357–382, 1985.

- [Jor00] À. Jorba. On practical stability regions for the motion of a small particle close to the equilateral points of the real Earth–Moon system. In J. Delgado, E.A. Lacomba, E. Pérez-Chavela, and J. Llibre, editors, *Hamiltonian Systems and Celestial Mechanics (HAMSYS-98)*, volume 6 of *World Scientific Monograph Series in Mathematics*, pages 197–213. World Scientific, 2000.
- [Jor01] À. Jorba. Numerical computation of the normal behaviour of invariant curves of n -dimensional maps. *Nonlinearity*, 14(5):943–976, 2001.
- [JV97a] À. Jorba and J. Villanueva. On the normal behaviour of partially elliptic lower dimensional tori of Hamiltonian systems. *Nonlinearity*, 10:783–822, 1997.
- [JV97b] À. Jorba and J. Villanueva. On the persistence of lower dimensional invariant tori under quasi-periodic perturbations. *J. Nonlinear Sci.*, 7:427–473, 1997.
- [JV98] À. Jorba and J. Villanueva. Numerical computation of normal forms around some periodic orbits of the Restricted Three Body Problem. *Phys. D*, 114:197–229, 1998.
- [JV01] À. Jorba and J. Villanueva. The fine geometry of the Cantor families of invariant tori in Hamiltonian systems. In *European Congress of Mathematics, Vol. II (Barcelona, 2000)*, volume 202 of *Progr. Math.*, pages 557–564. Birkhäuser, Basel, 2001.
- [KO98] B. Krauskopf and H. Osinga. Globalizing two-dimensional unstable manifolds of maps. *Internat. J. Bifur. Chaos Appl. Sci. Engrg.*, 8(3):483–503, 1998.
- [Mee85] J. van der Meer. *The Hamiltonian Hopf bifurcation*, volume 1160 of *Lecture Notes in Math.* Springer, New York, 1985.
- [Mey98] K.R. Meyer. The evolution of the stable and unstable manifold of an equilibrium point. *Celestial Mech.*, 70:159–165, 1998.
- [MH92] K.R. Meyer and G.R. Hall. *Introduction to Hamiltonian Dynamical Systems and the N -Body Problem*. Springer, New York, 1992.
- [Oll00] M. Ollé. Numerical exploration of bifurcation phenomena associated with complex instability. In *Numerical methods for bifurcation problems and large-scale dynamical systems (Minneapolis, MN, 1997)*, volume 119 of *IMA Vol. Math. Appl.*, pages 319–326. Springer, New York, 2000.
- [OP98a] M. Ollé and J.R. Pacha. Dynamics and bifurcation near the transition from stability to complex instability: some examples. In *Actas del XV CEDYA / V CMA*, pages 339–344. Universidad de Vigo, 1998.
- [OP98b] M. Ollé and D. Pfenniger. Vertical orbital structure and the Lagrangian points in barred galaxies. *Astron. Astrophys.*, 334:829–839, 1998.

- [OP99a] M. Ollé and J.R. Pacha. The 3d elliptic RTBP: periodic orbits which bifurcate from limiting restricted problems: complex instability. *Astron. Astrophys.*, 351:1149–1164, 1999.
- [OP99b] M. Ollé and D. Pfenniger. Bifurcation at complex instability. In C. Simó, editor, *Hamiltonian Systems with Three or More Degrees of Freedom*, NATO Adv. Sci. Inst. Ser. C Math. Phys. Sci., pages 518–522. Held in S’Agaró, Spain, 19–30 June 1995. Kluwer Acad. Publ., Dordrecht, Holland, 1999.
- [OPV] M. Ollé, J.R. Pacha, and J. Villanueva. Dynamics and bifurcation near the transition from stability to complex instability. To appear in the *Proceedings of the IV International Symposium HAMSYS-2001*, held in Guanajuato (México), March 19–24, 2001.
- [Pac02] J.R. Pacha. *On the quasi-periodic Hamiltonian Andronov-Hopf bifurcation*. PhD thesis, Universitat Politècnica de Catalunya, 2002.
- [Pfe85a] D. Pfenniger. Numerical study of complex instability. I mappings. *Astron. Astrophys.*, 150:97–111, 1985.
- [Pfe85b] D. Pfenniger. Numerical study of complex instability. II barred galaxy bulges. *Astron. Astrophys.*, 150:112–128, 1985.
- [Pfe90] D. Pfenniger. Stability of the Lagrangian points in stellar bars. *Astron. Astrophys.*, 230:55–66, 1990.
- [Sim94] C. Simó. Averaging under fast quasiperiodic forcing. In J. Seimenis, editor, *Hamiltonian Mechanics: Integrability and Chaotic Behaviour*, volume 331 of *NATO Adv. Sci. Inst. Ser. B Phys.*, pages 13–34. Held in Toruń, Poland, 28 June–2 July 1993. Plenum, New York, 1994.